Structure of the amorphous, massive-metallic-glass forming $Ni_{25}Zr_{60}Al_{15}$ alloy from molecular dynamics simulations

M. Guerdane* and H. Teichler†
Institut für Materialphysik, Universität Göttingen, D-37073 Göttingen, Germany
(Received 13 July 2001; published 3 December 2001)

Results are reported from molecular-dynamics simulations on the structure of the amorphous, massive-metallic-glass forming $Ni_{25}Zr_{60}Al_{15}$ alloy. The applied atomic-interaction model predicts radial distribution functions for the glass and specific-heat values for the melt that fit well to the experimental data in the literature. Analysis of bond-angle distribution and nearest-neighbor numbers reveal two types of short-range order in the system, related to the environments of Al and of Ni atoms. While Ni atoms have a trigonal prismatic neighbor shell under avoidance of direct Ni-Ni contacts, the Al atoms show an icosahedral surrounding with a tendency to form short segments of Al chains. It is the particular feature of the ternary alloy that its structure has to simultaneously accommodate both types of ordering. Even at high temperatures, the local order leads to prepeaks in the Ni and Al structure factors that experimentally should be detectable in the melt above the equlibrium melting point.

DOI: 10.1103/PhysRevB.65.014203 PACS number(s): 81.05.Kf, 52.65.Yy

I. INTRODUCTION

Although in the last decade a large amount of experimental work has been devoted to the study of the multicomponent ''bulk-metallic-glass'' forming alloys,[1–7] the microscopic details of these exceptional new materials are still an open question. In order to advance on the atomic scale, the basic understanding of the special properties of this novel class of amorphous alloys with their interesting technological perspectives, we present here results from molecular-dynamics (MD) simulations for one representative of this class. MD simulations have been used successfully to analyze the structural, thermodynamic, and dynamic properties of simple and binary amorphous alloys at a microscopic level on a scale ranging from the vibration (1 ps) to the mesoscopic (1 μs) times.[8–13] For metallic glasses with more than two components, only a few computer studies have been performed so far, e.g., for $Ga_{15}Zn_{15}Mg_{70}$.[14] Here we report results of MD simulations on the thermodynamic and structural properties of the ternary amorphous alloy $Ni_{25}Zr_{60}Al_{15}$,[15] which experimentally[1] has a large glass-forming ability (GFA) and belongs to the bulk amorphous alloys. According to our best knowledge, this is the first MD simulation dealing with a ternary bulk-metallic-glass model system.

Experimentally, amorphous Ni-Zr-Al ternary alloys were developed first by Inoue *et al.*[1] They exhibit a wide supercooled-liquid region and a high mechanical strength at the Zr-rich composition side. In particular, the composition $Ni_{25}Zr_{60}Al_{15}$ has a wide span between crystallization and glass-transition temperature, $\Delta T_x = T_x - T_g \approx 80$ K, which is the largest for this class of amorphous alloys. Therefore, we selected this particular composition for our study. The highest value of the reduced glass transition temperature is also found in the vicinity of this composition, with $T_g/T_m \approx 0.64$.

The present contribution is devoted to the analysis of the structural details of a ternary-alloy model and its possible differences to Zr-rich binary $Ni_{1-x}Zr_x$ systems. The analysis shows that in the ternary system two types of chemical short-range order (SRO) prevail, related to the Al and the Ni subsystems. It is the particular feature of the ternary alloy that it has to accommodate simultaneously both types of structural order, while the binary systems show only one type each.

The particular order in the ternary $Ni_{25}Zr_{60}Al_{15}$ model is reflected in its medium range order (MRO). MRO in liquids and amorphous solids has attracted increasing interest recently[16–19] as it refers to the existence of structural order on a scale larger than the average nearest-neighbor distance. MRO gives rise to the so-called first sharp diffraction peak (FSDP) in the structure factor $S(Q)$ at a Q value smaller than that of the main peak where the latter commonly is associated with SRO. Our structural analysis reveals the existence of well-defined FSDP's in the partial Faber-Ziman structure factors $S^{FZ}_{NiNi}(q)$ and $S^{FZ}_{AlAl}(q)$, a clear signature for ordering beyond the nearest-neighbor distance. Below, aspects of this order are described as visible in the bond-angle distribution, the pair distribution functions, the structure factors, and the stress distribution around the atoms.

In the literature, MRO is attributed to various mechanisms. In the case of the network-forming ''strong'' glasses (for the classification see Angell[20]), the FSDP is related to the network structure following from the directional covalent bonding or the ionic-polarization effects (e.g., Refs. 19 and 21). FSDP's have been also observed in some ''fragile'' glasses.[22–24] In this case the MRO is attributed to the formation of structural units constituted of unlike atoms (good mixing behavior) or like atoms (demixing tendency). The MRO in this case could be dictated by steric conditions (topological order) or by chemical affinities between the different atoms (chemical order). These two orders are not necessarily independent of each other. A further interpretation of the FSDP is the void-based approach used by Sadigh *et al.*[18] to explain the MRO in a simple monoatomic liquid simulated by MD methods.

As described below, our studies show that in the ternary

$Ni_{25}Zr_{60}Al_{15}$ alloy the FSDP's are induced by well-described chemical- and atom-size-related ordering effects in the melt and in the amorphous solids. The simulations predict that this structural order develops already at very high temperatures, well above equilibrium melting point, and thus should be experimentally detectable in the melt. In a study of a selected group of Zr-based bulk metallic glasses, Busch *et al.*[25] relate the large GFA of these materials to the presence of a comparable chemical order in the melt.

The paper is organized as follows. In the following section some details of the potentials used in this investigation are described. A thermodynamic study is given in Sec. III A. Calculated structure data are compared with available experimental data in Sec. III B. In Sec. III C, an insight in the topological ordering is given by analyzing the bond-angle distribution. The medium range order is discussed in Sec. III D. Some concluding remarks are added at the end.

II. MODEL AND METHOD

The MD calculations are carried out as isothermal-isobaric (N,T,p) simulations for an orthorhombic basis cell containing $N=1100$ atoms with cyclic boundary conditions. The equations of motion of the N particles at temperature T and (zero) external pressure p are numerically integrated by a fifth-order predictor-corrector algorithm with time step Δt_0 typically 2.5×10^{-15} s. Temperature here is introduced as the kinetic temperature determined from suitable time averages of the kinetic energy.

Well-relaxed structures are generated by cooling and equilibrating the system, starting with a liquid configuration at 3000 K. The equilibration time lies between about 0.8×10^6 integration steps (2 ns) at highest temperatures and 20×10^6 integration steps (50 ns) at lowest temperatures. In order to evaluate the various physical parameters, data analysis is carried out over about the last two-thirds of the equilibration run. Taking into account the equilibration time, the effective cooling rate is of the order of 10^{10}-10^9 K/s.

In order to model the interatomic couplings of the binary Zr-rich $Ni_{1-x}Zr_x$ reference systems, we follow the approach from Refs. 8 and 9 using short-ranged pair potentials, aimed at taking care of the electronic *d*-state interactions, and a volume-dependent *s*-state part $E_{Vol}(V)$. For the pair potentials $\Phi_{IJ}(r)(I,J\in\{Ni,Zr\})$ an expression of a slightly generalized Stillinger-Weber (SW) form[26] is used,

$$\Phi_{ij}(r)=A[(\alpha r-a_1)^{-n}-1]\exp\left(\frac{1}{\alpha r-a_2}\right)\quad (r<a_2/\alpha). \tag{1}$$

For estimating the pair-potential parameters, we combine information from the Hausleitner-Hafner hybridized nearly free-electron tight-binding-bond model[27] for $Ni_{35}Zr_{65}$ with experimental data about the partial distribution functions of amorphous $Ni_{35}Zr_{65}$ (Ref. 22) and its particle density. In Table I are given the SW parameters for the NiZr-system used here.

In order to model the ternary $Ni_{25}Zr_{65}Al_{15}$ alloy for the Ni-Zr subset, the above-described pair potentials for the disordered binary alloy $Ni_{35}Zr_{65}$ are adopted. Regarding the Al coupling, $\Phi_{\text{Al-Al}}$ is described by the pair potential suggested by Pettifor and Ward[28] for pure Al within the framework of second-order pseudopotential theory,[29]

$$\Phi(r)=2\frac{Z^2}{r}\sum_{n=1}^{3}A_n\cos(k_nr+\alpha_n)e^{-\kappa_nr}, \tag{2}$$

with values given in Table II. As this potential is of a long-range nature due to the asymptotic Friedel oscilllations, we impose a cutoff radius at a distance of 5.5 Å.

For the remaining cross-interaction potentials $\Phi_{\text{Ni-Al}}$ and $\Phi_{\text{Zr-Al}}$, we assume the empirical Stillinger-Weber form, Eq. (1). The parameters of the potentials are deduced by fitting to the experimental values of the cohesive energy E_c, the bulk modulus B and the lattice constants of the crystalline $L1_2$ structures Ni_3Al and Zr_3Al. The experimental value of the bulk modulus of Zr_3Al is not available in the literature, to our knowledge. We used, therefore, a value of 0.62 eV Å^{-3} determined by Spangenberg[30] in a first-principles linear muffin-tin orbital (LMTO) calculation, which is close to the concentration-weighted average of the bulk moduli of pure Zr (Ref. 31) and Al,[32] 0.58 eV Å^{-3}.

Table I presents SW parameters obtained by standard fit routines,[33] which describe well the input quantities under the assumption of a short-ranged potential. Table III compiles the experimental values of the input quantities and their calculated counterparts from the SW parameters.

In each subset (Ni-Zr, Ni-Al, and Zr-Al) the interaction energy between the pair of unlike atoms is found to be lower than the mean interaction energy in like-atom pairs

$$\Phi(r_{AB})<\frac{1}{2}\left|\Phi(r_{AA})+\Phi(r_{BB})\right| \tag{3}$$

for r_{ij}, the potential minimum distances. This means a compound-formation tendency or a heterocoordination preference in the three binary subsets.[29] This trend is experimentally well established for the binary compounds as reflected

TABLE I. Stillinger-Weber potential parameters [Eq. (1)] used for the atom pairs indicated in the table.

	A (eV)	α(Å^{-1})	a_1	a_2	n
Ni-Ni	1.150	0.417	0	1.527	5
Ni-Zr	3.350	0.387	−0.135	1.665	5
Zr-Zr	5.166	0.337	−0.025	1.829	3
Ni-Al	3.060	0.429	0	1.717	3
Zr-Al	1.305	0.339	−0.068	1.830	12

TABLE II. Pair-potential parameters [Eq. (2)] for pure Al after Pettifor and Ward (Ref. 28).

n	A_n (eV)	k_n(Å)	κ_n(Å)	α_n/π
1	57.317	0.546	2.776	−0.441
2	9.176	2.254	2.443	0.832
3	0.216	3.353	0.977	0.431

TABLE III. Experimental values of Ni_3Al and Zr_3Al properties used in the fit of the parameters of the Stillinger-Weber pair potentials $\Phi_{Ni\text{-}Al}$ and $\Phi_{Zr\text{-}Al}$, respectively.

	Ni_3Al		Zr_3Al	
	Expt.	Calc.	Expt.	Calc.
a(Å)	3.57 [a]	3.54	4.37 [b]	4.38
E_c (eV)	4.57 [a]	4.45	5.89 [c]	5.90
B(eV Å^{-3})	1.03 [a]	1.05	0.62 [d]	0.65

[a]Reference 32.
[b]Reference 34.
[c]Reference 35.
[d]Reference 30, determined by Spangenberg using first-principles LMTO calculation.

by a pronounced negativity of their respective heats of mixing and a strong tendency to short-range order in their structure.[22,35,36] The heterocoordination seems to be stronger for the binary systems Ni-Al and Ni-Zr than for Zr-Al. This feature implies that there may be a competing mechanism in the chemical short-range order in the ternary alloy Ni-Zr-Al.

III. RESULTS

A. Enthalpy and specific heat

In this section, we report results of the simulations concerning thermodynamic quantities of the binary and ternary model. Figure 1 presents the enthalpy per atom reduced by the energy of the harmonic oscillator, $H-3k_BT$, as a function of temperature. Experimentally and from MD simulation, this quantity is found to undergo significant changes in the glass-transition region, which commonly are interpreted in the way that the system falls out of equilibrium below T_g. The changes manifest themselves in our simulations at the temperature $T\approx 1050$ K for the ternary and at $T\approx 1200$ K for the binary $Ni_{40}Zr_{60}$ alloy. We identify these temperatures as the caloric glass temperatures for the corresponding model.

Since in our case the cooling rates in both cases are comparable, the higher T_g for the binary system suggests, thus, that there structural relaxations take place more slowly than

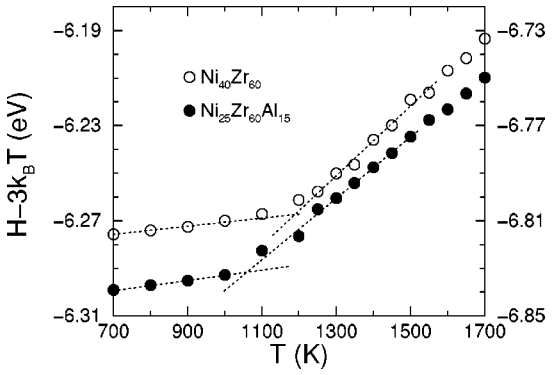

FIG. 1. Enthalpy $H-3k_BT$ per particle versus temperature T for the ternary $Ni_{25}Zr_{65}Al_{15}$ and binary $Ni_{40}Zr_{60}$ alloys.

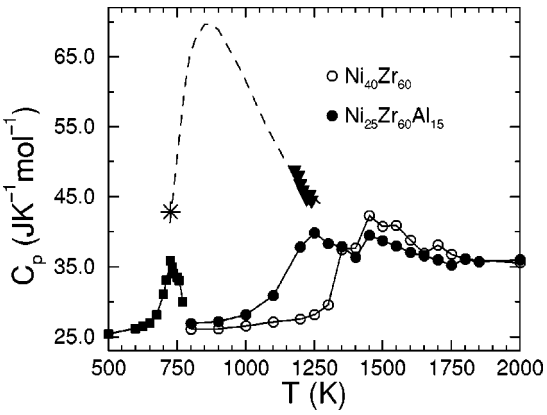

FIG. 2. Specific heat C_p versus temperature T for the ternary $Ni_{25}Zr_{65}Al_{15}$ and binary $Ni_{40}Zr_{60}$ alloys as calculated from our model (circles). The experimental results are measurements in the glassy state (full squares) (Ref. 1) and in the undercooled liquid (triangles and star) (Refs. 39 and 40). The dashed line is calculated C_p (Ref. 40) using the associate model.

in the ternary system. This reflects slower atomic dynamics in the binary model or a reduced probability for transitions into altered configurations, in the spirit of the potential-energy-landscape picture.

By differentiating the enthalpy H with respect to the temperature, we obtain the specific heat at constant pressure C_p. C_p can be, alternatively, evaluated from the time-average fluctuations of the enthalpy at a given temperature,[37,38]

$$\langle(\delta H)^2\rangle=\langle H^2\rangle-\langle H\rangle^2=k_BT^2C_p. \tag{4}$$

The validity of this formula supposes that the system is in thermodynamic equilibrium. Use of Eq. (4) is particularly favorable when the enthalpy data are spoilt by noise or not sufficiently precise to allow the evaluation of the derivative.

The values of C_p at temperatures above T_g are calculated here by using the fluctuation formula (4). For temperatures below T_g, this formula turns out to underestimate C_p, which is probably due to the fact that for $T<T_g$ the simulation time scale is too short to describe all possible fluctuations of the system. Therefore, we evaluated C_p in this temperature range from the direct differentiation of the enthalpy. The results are displayed in Fig. 2. There also are included the experimental results $C_{p,exp}$ from the differential scanning-calorimetry (DSC) measurements for the amorphous $Ni_{25}Zr_{65}Al_{15}$ alloy by Inoue *et al.*,[1] for the undercooled melt by Zappel and Sommer[39] and for the melt by Zhou and Sommer.[40] Additionally we show in Fig. 2 the interpolation curve deduced by Zhou and Sommer[40] for the undercooled melt in the framework of their associate model. Our MD-simulation data extrapolate quite well experimental data to higher temperatures, indicating that our model describes sufficiently well the density of states in the equilibrium melt.

At very low temperatures, the experimental and the calculated values of C_p tend both to the classical Dulong-Petit value expected for a harmonic solid ($C_p\approx 25$ JK^{-1}g^{-1}).

The experimental glass temperature $T_{g,expt}$ from DSC heating measurements for the binary $NiZr_2$ and the ternary $Ni_{25}Zr_{65}Al_{15}$ alloy are around 652 K (Ref. 41) and 720 K,[1]

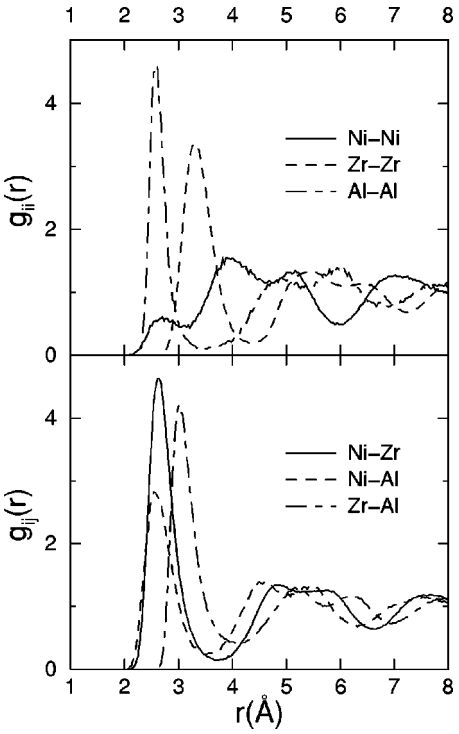

FIG. 3. Partial pair-correlation functions $g_{ij}(r)$ of $Ni_{25}Zr_{65}Al_{15}$ at $T=300$ K.

respectively. These data are well below the values of our calculations, 1200 K for the binary and 1050 K for the ternary system determined from the bend in the energy data. The deviations can be partly attributed to the cooling-rate dependence of T_g. The cooling rate used in our MD simulations ($\approx 10^{10}$ K/s) lies at least 4 decades above typical cooling rates used in experiments ($<10^6$ K/s for conventional glasses and $<10^2$ K/s for bulk amorphous alloys) and about 8–10 decades above typical heating rates of DSC measurements (≈ 10 K/s). For the binary system, nevertheless, a more detailed comparison of calculated and experimental T_g is possible. From heating experiments on $Ni_{34}Zr_{66}$, Lück *et al.*[42] deduced a raise of the glass temperature to about 942 K for a heating rate of 10^{12} K/s. Furthermore, in Ref. 12 it was established that for the simulation model of $Ni_{50}Zr_{50}$ based on Hausleitner-Hafner potentials the calculated melting temperature has to be reduced by about 21% to get the experimental one. Assuming that the same overestimation holds for T_g in $Ni_{40}Zr_{60}$, yields a reduced $T_{g,red}\approx 950$ K, which surprisingly well compares to the estimate of Lück *et al.*

B. Radial distribution functions

Figure 3 shows the calculated partial pair-correlation functions $g_{ij}(r)$ in the glassy state at $T=300$ K. Table IV displays the nearest-neighbor numbers z_{ij} deduced therefrom by integrating the partial densities up to the first minimum in the radial distribution function.

$g_{\text{Ni-Ni}}(r)$ exhibits only a weak nearest-neighbor peak, which becomes smaller with decreasing temperature. The first peak in $g_{\text{Ni-Zr}}(r)$ is very intense, even more than that of the Zr-Zr distribution. This manifests the tendency for Ni atoms to be preferentially surrounded by Zr as nearest neighbors. Such an ordering between Ni and Zr atoms has been already observed experimentally[22,43] and confirmed theoretically[23] in binary Ni-Zr alloys, and is attributed to the strong negative heat of mixing or the pronounced nonadditivity of the pair potentials as argued by Hausleitner and Hafner.[23]

TABLE IV. Nearest-neighbor distances d_{ij} and coordination numbers z_{ij} in amorphous $Ni_{25}Zr_{60}Al_{15}$. The experimental results are from measurements of Matsubara and Waseda (Ref. 44).

	d_{ij}(Å) (calc.)	d_{ij}(Å) (expt.)	z_{ij} (calc.)	z_{ij} (expt.)
Ni-Ni	2.65		0.50	
Zr-Ni	2.63	2.67	3.02	2.2
Ni-Zr	2.63	2.67	7.25	
Zr-Zr	3.30	3.17	9.93	10.3
Ni-Al	2.60		1.20	
Al-Ni	2.60		2.00	
Zr-Al	3.02		2.25	0.0
Al-Zr	3.02		8.99	
Al-Al	2.59		1.06	

In the subsystem Zr-Al, the pronounced first peak and first minimum in $g_{\text{Al-Al}}(r)$ deserves particular attention. While the peak has a marked height, its integrated intensity, that is $z_{\text{Al-Al}}$, is around 1. This value, on the one hand, reflects suppression of direct Al-Al contacts below the value 1.8 following from random Al distribution. On the other hand, the peak height indicates that the remaining Al-Al pairs have a rather narrow distance distribution. Closer inspection of the MD data reveals for the Al atoms a tendency to form short, linear-chain segments, as visible in the snapshot in Fig. 4. This latter observation implies the existence of an appropriate number of isolated Al atoms with regard to the low $z_{\text{Al-Al}}$.

As already mentioned, the three binary systems Ni-Zi, Ni-Al, and Zr-Al show good compound-forming behavior. It is obvious that the final structure of the ternary system $Ni_{25}Zr_{60}Al_{15}$ is determined by the competition of the mixing ability of the binary subsystems. The bonding strengths of the two minority species Ni and Al to the majority species Zr is of particular importance here. Since the compound-forming tendency of Ni-Zr seems to be stronger than that of Al-Zr, it is expected that Al-Zr heterocoordination will be weakened by the stronger Ni-Zr preference. From that, an Al-Al clustering tendency can be inferred. The atom-size effect may be an additional cause for the formation of Al chains. Moreover, Ni atoms, with their small size, are more appropriate than Al atoms to match into the Bernal holes of the Zr matrix. Total demixing into Al clusters is, nevertheless, hindered by the marked Al-Zr and strong Ni-Al heterocoordination.

From the partial coordination numbers z_{ij} in Table IV, total coordination numbers can be deduced, yielding $N_{\text{Ni}} \approx 9$, $N_{\text{Zr}}\approx 15$, and $N_{\text{Al}}\approx 12$. The values for Ni and Zr are close to the estimates known from simulations for the Zr-rich amorphous $Ni_{1-x}Zr_x$ alloys.[23] In contrast to this, the value of

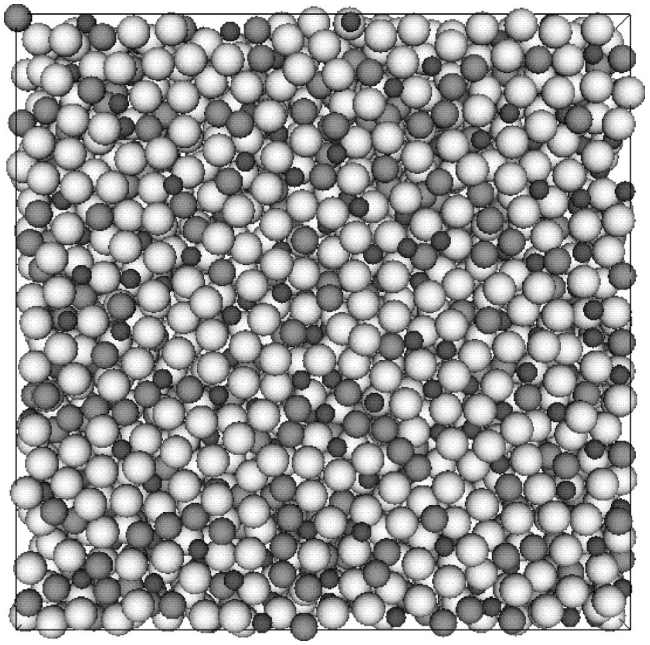

FIG. 4. Cross section of a simulated amorphous $Ni_{20}Zr_{65}Al_{20}$ configuration at 800 K. (Large light spheres, Zr; small dark, Ni; intermediate gray, Al. Box length ≈ 60 Å.)

N_{Al} indicates for these species a novel type of atomic environment, not present in the binary systems. Regarding the z_{ij} in Table IV, good agreement is found in case of $z_{\mathrm{Zr\text{-}Ni}}$ and $z_{\mathrm{Zr\text{-}Zr}}$ when comparing the experimental estimates by Matsubara and Waseda[44] with our MD-simulated values. There seems a significant difference in the numbers $z_{\mathrm{Zr\text{-}Al}}$ from experiment and simulation. Considering the enormous difficulties to extract $z_{\mathrm{Zr\text{-}Al}}$ from the experiments, this discrepancy, however, should not be considered as too serious.

The atomic structure of $Ni_{25}Zr_{65}Al_{15}$ amorphous alloy was investigated exprimentally by Matsubara and Waseda,[44] who used anomalous x-ray scattering (AXS) in combination with the ordinary x-ray diffraction to determine the ordinary and the environmental radial distribution functions (RDF). The results of these measurement are reproduced in Fig. 5 together with the calculated RDF from our MD simulations.

The curves at the top of Fig. 5 correspond to the ordinary RDF's that represent the radial distribution around the average atom, independently of the atom species. It is the weighted sum of the six partial pair-correlation functions $g_{ij}(r)$,

$$4\pi r^2\rho(r)=4\pi r^2\sum_{i,j}\sum_{=\mathrm{Zr,Ni,Al}}\frac{c_i f_i f_j}{\langle f\rangle^2}g_{ij}(r), \tag{5}$$

with $\langle f\rangle=\Sigma_i c_i f_i$. c_i and f_i are the atomic concentration and the atomic scattering factor of the element *i*, respectively.

The curves at the center and the bottom of Fig. 5 correspond to the environmental RDF's for Zr and Ni, respectively. The experimental curves have been determined by the AXS method. The environmental RDF provides the weighted average over all atomic pairs around a given element *A*

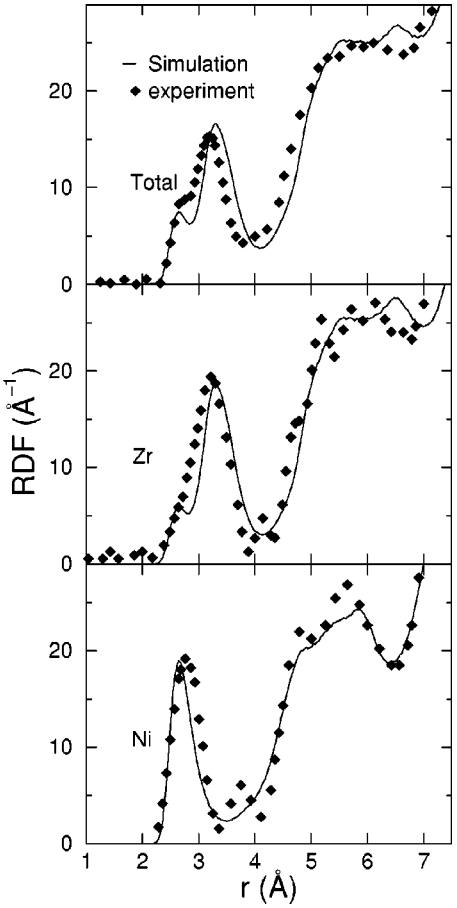

FIG. 5. The ordinary (top) and environmental RDF's for Zr (center) and Ni (bottom) of $Ni_{25}Zr_{65}Al_{15}$ amorphous alloy at 300 K. Calculated (solid line) and measured (filled diamond) data are compared. The experimental results are measurements of Matsubara and Waseda (Ref. 44).

$$4\pi r^2\rho_A(r)=4\pi r^2\sum_{i=\mathrm{Zr,Ni,Al}}\frac{\mathrm{Re}[f_i(E_1)+f_i(E_2)]}{W(E_1,E_2)}g_{Ai}(r), \tag{6}$$

$$W(E_1,E_2)=\sum_i c_i\mathrm{Re}[f_i(E_1)+f_i(E_2)], \tag{7}$$

where f_i is the total x-ray atomic-scattering factor, a complex number that contains an anomalous dispersion term in addition to the usual atomic-scattering factor. The measurements have been carried out at two energies E_1 and E_2 below the absorption edge of the considered atom. Re denotes the real part of the values in the brackets. For more details we refer to Ref. 44.

Figure 5 demonstrates that qualitatively as well as quantatively the experimental and the calculated curves agree well. The height and the location of the peaks are sufficiently reproduced. The peaks positions, as given in Table IV, are found to be within 4% of the values obtained by Matsubara and Waseda. However, the splitting of the first peak in the calculated RDF of Zr is somewhat larger than the measured one, where the latter shows only a weak hump at the same location (note that this hump becomes more and more impor-

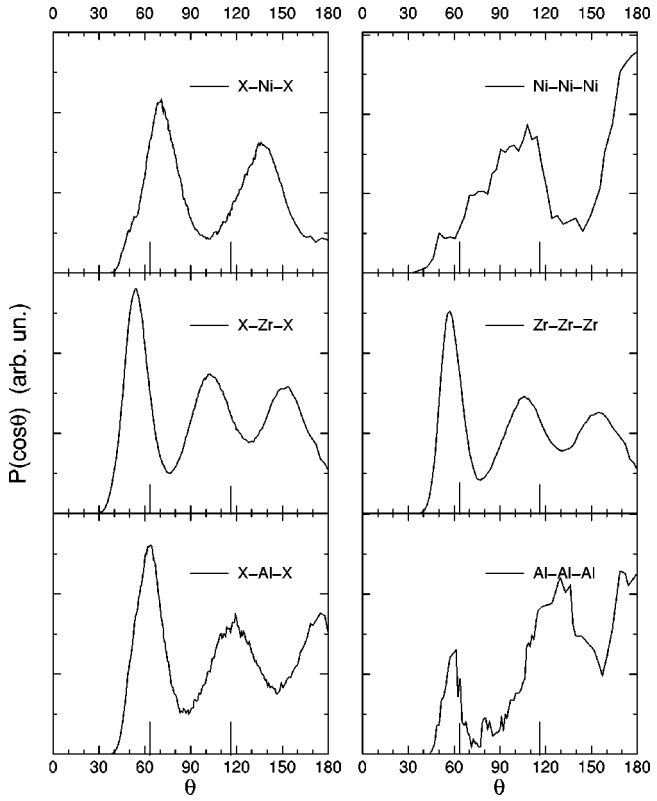

FIG. 6. Partial bond-angle distributions in amorphous $Ni_{25}Zr_{60}Al_{15}$ alloy. *X* means that all atom species are considered. The vertical lines indicate the bond angles in a regular icosahedron ($\theta = 63.5, 116.5, 180$).

tant with annealing and crystallization[44]). The hump represents the Ni-Zr correlation whereas the main peak results from Zr-Zr correlations. The discrepancy reflects the fact that our model slightly underestimates the Ni-Zr interatomic distance and simultaneously overestimates the Zr-Zr one, as can be seen from Table IV.

C. Bond-angle distribution

A first insight in the topological order present in the structure of $Ni_{25}Zr_{65}Al_{15}$ can be obtained from the distribution function of the bond angles around each atom species. This triple-correlation function is defined as an average of bond angles between a reference atom and the pairs of atoms within a radius R_{max}, choosen here as the first minimum of the total radial correlation function $g_{tot}(r)$, $R_{max} \approx 4.1$ Å. The results of this analysis are displayed in Fig. 6.

The distributions of the angles formed by bonds centered at the Zr and Ni sites present the same features as those calculated by Hausleitner and Hafner[23] for the binary systems $Ni_{50}Zr_{50}$ and $Ni_{33}Zr_{67}$. In (Ref. 23) it is pointed out that the peaks in these angular correlations are compatible with a local trigonal-prismatic order similar to that in the crystalline CrB (*B*33) structure. Patterns of other trigonal-prismatic structures, like Fe_3C, are also detected in the binary systems.[23] In CrB-type compounds, like NiZr, the trigonal prisms form layers with B(Ni) atoms centering the prisms. The B(Ni) atoms being arranged in zigzag chains within this configuration.

Interpreting the here deduced bond-angle distributions in the light of the picture advanced by Hausleitner and Hafner,[23] the bond angles centered at Zr sites correspond to those on the triangular and square faces of a prism ($\theta \approx 60°$, $\theta \approx 90° - 100°$) and to the rotation of two edge-sharing prisms ($\theta \approx 145°$) (like in a Fe_3C structure). The bond angles centered at Ni sites, $\theta \approx 75°$ and $\theta \approx 135°$, correspond to angular correlations between a Ni atom centering on the prism and two other atoms on the vertices. The vertices are occupied in this model by Zr atoms predominantly. The pronounced peak at $\theta \approx 110°$ in the Ni-Ni-Ni angular correlation is very close to the chain angle of $\theta = 110°$ in the CrB structure.

The distribution of the bond angles at Al sites shows a different pattern than those around Zr or Ni sites. It exhibits well-defined peaks at $\theta \approx 60°$, $\theta \approx 120°$, and $\theta \approx 180°$, which are very close to the icosahedral bond angles ($\theta \approx 63.5°$, $\theta \approx 116.5°$, and $\theta \approx 180°$). This suggests that Al atoms occupy sites with a predominantly icosahedral symmetry, in contrast to Ni atoms that occupy sites with trigonal-prismatic symmetry. The coordination numbers $N_{Ni} \approx 9$ for Ni and $N_{Al} \approx 12$ for Al (see Table IV) are compatible with this assumption too.

D. Static structure factors and medium-range order

The partial Faber-Ziman (FZ) structure factor is defined as the Fourier transform of the partial RDF (Ref. 45)

$$S_{ij}^{FZ}(k) = 1 + \rho_0 \int 4\pi r^2 [g_{ij}(r) - 1] \frac{\sin(kr)}{kr} dr, \qquad (8)$$

where ρ_0 is the averaged number density of the *i*-*j* subsystem. The results are displayed in Fig. 7.

The FZ structure factors of the binary $Ni_{40}Zr_{60}$ and ternary $Ni_{25}Zr_{65}Al_{15}$ systems are on the whole very similar, except that the main peak of $S_{Zr\text{-}Zr}^{FZ}(q)$ is broader in the case of the binary system. For both systems $S_{Ni\text{-}Ni}^{FZ}(q)$ exhibits a well-defined prepeak at the left of the main peak, corresponding to the nearest-neighbor peak in $g_{Ni\text{-}Ni}(r)$. The prepeak at the wave vector $q \approx 1.9$ Å^{-1} seems to result from a correlation on a length scale of about 3.3 Å, after the conventional relation, $l = 2\pi/q$. The main peak, at the wave vector $q \approx 2.8$ Å^{-1}, corresponds to a length of $l \approx 2.3$ Å. This later value is, however, clearly smaller than the location of the first peak in $g_{Ni\text{-}Ni}(r)$ (about 2.7 Å), which shows that the conversion relation above gives underestimated length values (by about 20%). This can be further confirmed in the case of Ni-Zr and Zr-Zr correlations. Taking into account this correction, we obtain in the case of the prepeak a correlation length of about 3.9 Å. It seems plausible to attribute this length to the first split of the second peak in $g_{Ni\text{-}Ni}(r)$. Furthermore the slight hump at the left end of the prepeak, which is independent of the truncation value used for the Fourier transform, correlates well with the second split. There is no prepeak in the structure factor $S_{Zr\text{-}Zr}^{FZ}(q)$.

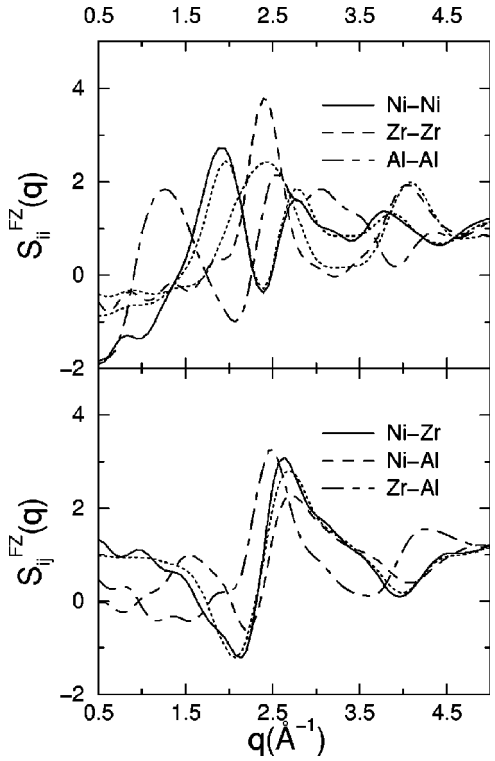

FIG. 7. Faber-Ziman structure factors $S_{ij}^{FZ}(q)$ of $Ni_{25}Zr_{65}Al_{15}$ at $T=300$ K. For comparison, the FZ structure factors of the binary $Ni_{40}Zr_{60}$ alloy are included by dotted lines.

The appearance of a prepeak in $S_{\text{Ni-Ni}}^{FZ}(q)$ reflects the existence of chemical medium-range order (CMRO) in the atomic configuration of the binary as well as the ternary system, in other words the preference for Ni atoms to be surrounded by Zr atoms, as discussed in Sec. III B.

In the subsystem Zr-Al, $S_{\text{Al-Al}}^{FZ}(q)$ also exhibits a well-defined prepeak at a wave vector $q\approx 1.3$ Å^{-1}, a clear signature of a structural order on a length scale of about 5.8 Å (corrected value). The peak related to the Al-Al nearest-neighbor distance is around $q\approx 2.6$ Å^{-1}, and shows an usual shoulder on the larger-q side.

Both prepeaks are associated with concentration fluctuations in the amorphous ternary system. The question how to describe these fluctuations in terms of atomic arrangements can be answered in the light of the results of the preceding two sections. In the picture of the trigonal-prismatic structural ordering (of the subsystem Ni-Zr), the location of the prepeak in the Ni-Ni correlation may be related to an average distance between neighboring trigonal prisms, where the Ni atoms occupy the centers of these prisms. This interpretation has been suggested by Suzuki *et al.*[24] for the prepeaks in the metal-metalloid amorphous alloys Pd-Ge and Pd-Si. The Al atoms are constrained to group into the space between these Ni-Zr units. According to Fig. 4, they apparently form predominantly linear-chain segments with a next nearest-neighbor distance of about 5.8 Å.

The temperature dependence of the prepeaks from the glassy state up to $T=5000$ K is displayed in Fig. 8. The intensity of both prepeaks increases continously upon cooling, marking thereby the increase of the structural ordering with decreasing temperature.

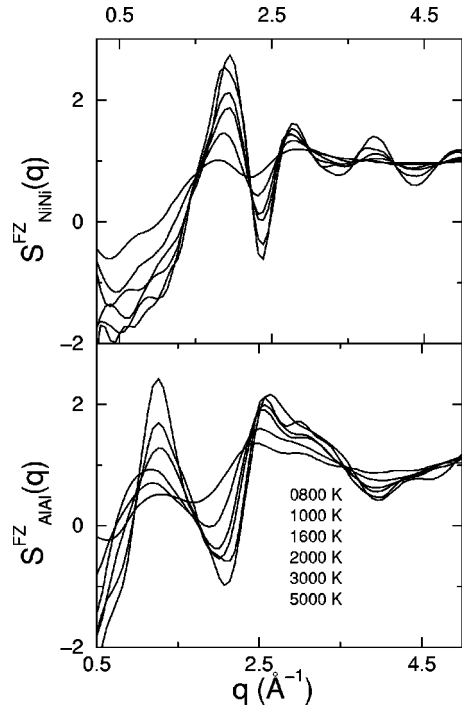

FIG. 8. Temperature dependence of the prepeaks associated with the Ni-Ni and Al-Al correlations. The indicated temperatures correspond to the sequence of the curves from the bottom to the top as given at the prepeak (first peak).

In the simulations the prepeaks are observed even at temperatures as high as $T=5000$ K, which indicates that the structural organization develops already at these very high temperatures. According to our results, the FSDP, as an indication of local order in the system, should be visible in an experimental structure analysis of the melt above the equilibrium melting temperature. The persistence of a well-defined MRO even far above the melting temperature seems to be a common feature of glass formers with bonding forces of covalent nature, like network-forming and transition-metals glassy systems.[21]

E. Atomic-level stress distribution

The approach of Egami *et al.*[46] allows to characterize the local atomic structure in the amorphous systems in terms of the distribution of internal stresses on the atomic level. The stress tensor acting at the atom i in a system of N atoms is given by

$$\sigma_i^{kl}=\frac{1}{\Omega_i}\left[m_i\mathbf{v}_i^k\mathbf{v}_i^l+\frac{1}{2}\sum_{j\neq i}^{N}\frac{\partial\Phi(\mathbf{r}_{ij})}{\partial\mathbf{r}_{ij}}\frac{\mathbf{r}_{ij}^k\mathbf{r}_{ij}^l}{\mathbf{r}_{ij}}\right],\quad k,l=1,2,3, \tag{9}$$

where $\mathbf{r}_i$ and $\mathbf{v}_i$ are the coordinates and the velocities, respectively, of the particle i, $\mathbf{r}_{ij}$ the vector joining particle i to particle j, and $\mathbf{F}_{ij}=-\partial\Phi(\mathbf{r}_{ij})/\partial\mathbf{r}_{ij}$ the force exerted by particle j on particle i. The summation extends over all the atoms within the cutoff radii of the potentials. Ω_i is the local atomic volume that can be identified with the volume of Wigner-Seitz cell of atom i, approximated as[46]

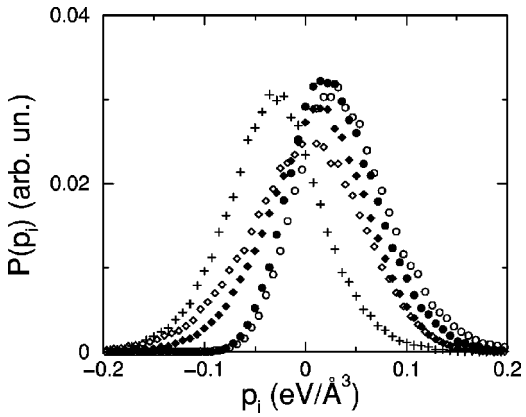

FIG. 9. Distribution of the atomic-level pressure in the ternary $Ni_{25}Zr_{60}Al_{15}$ (full symbols) and the binary $Ni_{35}Zr_{65}$ (open symbols) alloys at $T=800$ K. Circles, Ni; diamonds, Zr; plus signs, Al.

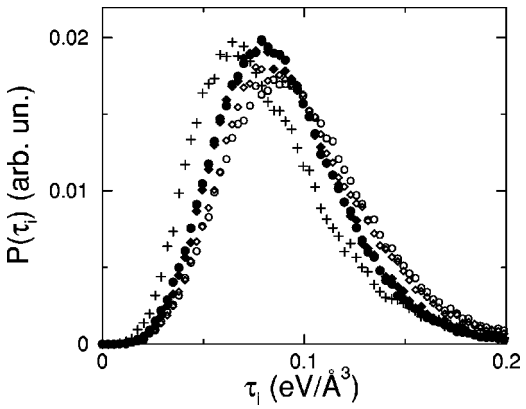

FIG. 10. Distribution of von Mises shear stress in the ternary $Ni_{25}Zr_{60}Al_{15}$ (full symbols) and the binary $Ni_{35}Zr_{65}$ (open symbols) alloys at $T=800$ K. Circles, Ni; diamonds, Zr; plus signs, Al.

$$\Omega_i^{1/3}=\frac{\sum_{j\in nn} r_{ij}^{-1}}{2\sum_{j\in nn} r_{ij}^{-2}}, \tag{10}$$

where the summation extends over the atoms within the nearest-neighbors (nn) shell of the atom i. In our case, we identify the nn shell with the volume of a sphere whose radius corresponds to the first minimum in the partial RDF $g_{ij}(r)$.

In analogy to the atomic pressure p_i

$$p_i=\frac{1}{3}\sum_{k=1}^{3}\sigma_i^{kk}, \tag{11}$$

the von Mises shear stress τ_i gives the magnitude of the shear stress at an atomic level independent of the coordinate system. τ_i is defined as[47]

$$\tau_i=\left\{\frac{1}{6}[(\sigma_i^{xx}-\sigma_i^{yy})^2+(\sigma_i^{yy}-\sigma_i^{zz})^2+(\sigma_i^{zz}-\sigma_i^{xx})^2]+(\sigma_i^{xy})^2 +(\sigma_i^{yz})^2+(\sigma_i^{zx})^2\right\}^{1/2}. \tag{12}$$

The distribution for the atomic-level pressure p_i is displayed in Fig. 9 and that for the shear stress τ_i in Fig. 10 for each species in the binary and the ternary systems at $T=800$ K. The pressure distribution averaged over all species is balanced by hydrostatic pressure due to the electron-gas term of the potential, E_{Vol}. The two distributions around Ni and Zr atoms show similar features in both systems. The pressure distribution around Ni is somewhat shifted to higher pressures with respect to the Zr distribution. According to the notation of Egami *et al.*,[46] the Ni sites are *p*-type interstitial-like defects (with higher-than-average densities). This observation provides support to the one discussed in Sec. III C about the existence of a pronounced topological order in both amorphous systems and to the fact that Ni atoms reside in the centers of well-defined optimally packed narrow structural units, in our case the trigonal prisma.

Striking in Fig. 10 is the large shift of the pressure distribution of Al to negative pressures, as well as the shift of the shear-stress distribution of the same species to lower shear stresses too. This attributes a *n*-defect vacancylike character to the Al sites (with lower-than-average densities). It follows therefrom that alloying of Al to the binary Ni-Zr melt introduces additional free volume in the system. The particular local symmetry and the specific stress distribution around the Al atoms reflect the fact that these atoms neither are a substitution for Ni nor for Zr when forming the ternary structure from the binary one. Alloying with Al clearly induces a significantly different, complex amorphous configuration.

IV. CONCLUDING REMARKS

Molecular-dynamics (MD) simulations have been used in this work to gain insights in the structural properties of the metallic-glass forming ternary alloy $Ni_{25}Zr_{60}Al_{15}$. The simulations are based on a model for interatomic couplings in terms of pair potentials and a global sp-electron-gas term.

Comparison of the calculated radial distribution functions (RDF) with the experimental results of Matsubara and Waseda[44] shows that the model reproduces the structural features of amorphous $Ni_{25}Zr_{60}Al_{15}$ with good accuracy. Good agreement with the experiments is also found regarding the specific-heat data. Our MD-simulation values extrapolate rather well to higher temperatures the measured data of Zhou and Sommer[40] and their interpolation in the associate model.

Analysis of the thermodynamics shows that the caloric glass-transition temperature T_g is shifted to lower temperatures by alloying Al to Ni-Zr alloy. Since in our case the cooling rates used for the binary and ternary systems are comparable, we conclude that the dynamical processes for a given temperature of the undercooled state are slower in the binary system than in the ternary one.

The structural analysis in Sec. III D reveals the existence of well-defined prepeaks in the Faber-Ziman structure factors $S^{FZ}_{\text{Ni-Ni}}(q)$ and $S^{FZ}_{\text{Al-Al}}(q)$. Both reflect the existence of pronounced chemical and topological medium-range order (MRO) in the system. The Ni prepeak is associated with the weak Ni-Ni coordination as can be seen from the anomalous

reduced first peak in $g_{\text{Ni-Ni}}$. The length related to the Ni prepeak is ≈ 3.9 Å and is associated with the second-nearest Ni-Ni pair correlation. The low nearest-neighbor number ($z_{\text{Ni-Ni}} \approx 0.5$) reflects the good mixing behavior in the binary Ni-Zr and Ni-Al subsystems, which makes the enthalpy of Ni-Ni pairs much more unfavorable than unlike pairs. Regarding Ni, the here observed features of the ternary system seem rather similar to those found by Hausleitner and Hafner[23] for the binary Ni-Zr melts from MD simulations and, e.g., Suzuki *et al.*[24] from neutron-scattering experiments.

The Al atoms on average have a coordination number of $N_{\text{Al}} \approx 12$ with an average Al-Al nearest-neighbor $z_{\text{Al-Al}} \approx 1$, which means that $z_{\text{Al-Al}}$ is well below the value 1.8 for random occupation of the neighbor sites. Despite the small average $z_{\text{Al-Al}}$, there is a tendency in the Al system to form short-chain segments as displayed by Fig. 4. They apparently give rise to the rather narrow range of Al-Al nearest-neighbor distances reflected by the sharp first peak in $g_{\text{Al-Al}}$. The prepeak in $S^{FZ}_{\text{Al-Al}}(q)$ corresponds to concentration fluctuations on a length scale of about ≈ 5.8 Å, which may be associated with intrachain next-nearest-neighbor distance.

A study of the bond-angle distribution in Sec. III C shows that the angular correlations at Ni and Zr sites are compatible with a local trigonal-prismatic order similar to that found in binary Ni-Zr alloys.[23] The Al atoms predominantly occupy sites with an icosahedral symmetry. This indicates that Al atoms have a local environment significantly different from that of Ni and Zr atoms. This finding is confirmed by the analysis of the atomic stress distribution, showing that Al atoms neither are a substitute for Ni nor for Zr when forming the ternary structure from the binary one.

The simulations predict that the prepeaks shall be observed even at temperatures as high as $T = 5000$ K. This indicates that the structural organization develops at temperatures well above the melting point. The persistence of a well-defined MRO even far above the melting temperature seems to be a common feature of glass formers with pure or partial covalent bonding, like network-forming and transition-metal glassy systems.[21] In a study on a selected group of Zr-based bulk metallic glasses, Busch *et al.*[25] relate the presence of such a chemical ordering in the melt with the large GFA of these materials. Atom-probe field-ion microscopy and small-angle neutron-scattering experiments show that this chemical ordering can result in clustering or phase separation.[48]

From the analysis of the short-range order we see that there are two different features in the ternary amorphous structure compared to the binary Ni-Zr system: First, there are two different types of local order around the Ni and the Al atoms which have to form the global complex-ordered structure of the amorphous alloy. Combination of two types of local order may give rise to a much larger variety of global structures than possible in a binary SRO melt or glass.

Secondly, while the Zr-rich binary amorphous alloys predominantly gives structure elements with nine nearest-neighbors atoms around Ni and more than 14 atoms around Zr, alloying by Al introduces elements with icosahedral symmetry and 12 neighbors on average. This may be of importance when interpreting the local structure within the polytetrahedral model[49] of the liquid (or glass). According to this model, icosahedra form the regular elements of the structure, while lower or higher coordination atoms are related to disclinations in the arrangement. Our finding thus means that addition of Al to the binary Ni-Zr amorphous alloy introduces regular structure elements to the system, definitely absent in the binary alloy.

ACKNOWLEDGMENTS

We aknowledge financial support from the DFG in the SPP: ''Unterkühlte Metallschmelzen - Phasenselektion und Glasbildung.''

*Email address: hamid@umpa06.gwdg.de
†Email address: teichler@umpa06.gwdg.de

[1] A. Inoue, T. Zhang, and T. Masumoto, Mater. Trans., JIM **31**, 177 (1990).
[2] A. Inoue, T. Zhang, and T. Masumoto, Mater. Trans., JIM **30**, 965 (1989).
[3] T. Zhang, A. Inoue, and T. Masumoto, Mater. Trans., JIM **32**, 1005 (1991).
[4] A. Peker and W.L. Johnson, Appl. Phys. Lett. **63**, 2342 (1993).
[5] E. Bakke, R. Busch, and W.L. Johnson, Appl. Phys. Lett. **67**, 3260 (1995).
[6] R. Busch, A. Masuhr, E. Bakke, and W.L. Johnson, Mater. Sci. Forum **269-272**, 547 (1998).
[7] A. Inoue, T. Zhang, and T. Masumoto, J. Non-Cryst. Solids **156-158**, 473 (1993).
[8] H. Teichler, Phys. Status Solidi B **172**, 325 (1992).
[9] H. Teichler, Phys. Rev. E **53**, 4287 (1996).
[10] H. Teichler, Phys. Rev. Lett. **76**, 62 (1996).
[11] B. Böddeker and H. Teichler, Phys. Rev. E **59**, 1948 (1999).
[12] H. Teichler, Phys. Rev. B **59**, 8473 (1999).
[13] H. Teichler, J. Non-Cryst. Solids **293-295**, 339 (2001).
[14] Z.H. Jin, K. Lu, Y.D. Gong, and Z.Q. Hu, J. Chem. Phys. **106**, 8830 (1997).
[15] M. Guerdane, Ph.D. thesis, Universität Göttingen, 2000.
[16] P. H. Gaskell, in *Proceedings of the 3rd International Conference on Rapidly Quenched Metals*, edited by B. Cantor (Metals Society, London, 1978), Vol. 2, p. 277.
[17] H. Iyetomi and P. Vashishta, Phys. Rev. B **47**, 3063 (1993).
[18] B. Sadigh, M. Dzugutov, and S.R. Elliott, Phys. Rev. B **59**, 1 (1999).
[19] L. Cormier, P.H. Gaskell, G. Calas, and A.K. Soper, Phys. Rev. B **58**, 11 322 (1998).
[20] C.A. Angell, Ann. N.Y. Acad. Sci. **371**, 136 (1981).
[21] J. Horbach and W. Kob, Phys. Rev. B **60**, 3169 (1999).
[22] T. Fukunaga, N. Hayashi, N. Watanabe, and K. Suzuki, in *Rapidly Quenched Metals*, edited by S. Steeb and H. Warlimont (Elsevier, New York, 1985), p. 475.
[23] Ch. Hausleitner and J. Hafner, Phys. Rev. B **45**, 128 (1992).
[24] K. Suzuki, T. Fukunaga, K. Shibata, T. Otomo, and H. Mizuseki, in *Thermodynamics of Alloy Formation*, edited by Y. A. Chang and F. Sommer (Minerals, Metals and Materials Society, Warrendale, PA, 1997).

[25] R. Busch, E. Bakke, and W.L. Johnson, Acta Mater. **46**, 4725 (1998).
[26] F.H. Stillinger and T.A. Weber, Phys. Rev. B **31**, 5262 (1985).
[27] Ch. Hausleitner and J. Hafner, J. Phys.: Condens. Matter **2**, 6651 (1990); Phys. Rev. B **45**, 115 (1992).
[28] D.G. Pettifor and M.A. Ward, Solid State Commun. **49**, 291 (1984).
[29] J. Hafner, *From Hamiltonians to Phase Diagrams*, Springer Series in Solid-State Sciences, Vol. 70 (Springer, Berlin, 1987).
[30] M. Spangenberg, Diploma thesis, Universität Göttingen, 1997.
[31] G. Simmons and H. Wang, *Single Crystal Elastic Constants and Calculated Aggregates Properties* (MIT Press, Cambridge, MA, 1971).
[32] S.P. Chen, A.F. Voter, and D.J. Srolovitz, Scr. Metall. **20**, 1389 (1986).
[33] *NAG Fortran Library Manual Mark* (NAG Central Office, Oxford, UK, 1980), Vol. 8, Chap. F01.
[34] *Pearson's Handbook of Crystallographic Data for Intermetallic Phases*, edited by P. Villars and L.D. Calvert (American Society for Metals, Metal Park, Ohio, 1986).
[35] *Cohesion in Metals*, edited by F.R. de Bor, R. Boom, W.C.M. Mattens, A.R. Miedema, and A.K. Niessen (North-Holland, Amsterdam 1988).
[36] M. Maret, T. Pomme, A. Pasturel, and P. Chieux, Phys. Rev. B **42**, 1598 (1990).
[37] L. D. Landau and E.M. Lifshitz, *Statistical Physics*, 3rd ed. (Pergamon, New York, 1980).
[38] J.R. Ray, Comput. Phys. Rep. **8**, 109 (1988).
[39] B.J. Zappel and F. Sommer, Mater. Sci. Eng., A **179/180**, 283 (1994).
[40] S.H. Zhou and F. Sommer, J. Non-Cryst. Solids **250-252**, 572 (1999).
[41] Z. Altounian, T. Guo-hua, and J.O. Strom-Olsen, J. Appl. Phys. **54**, 3111 (1983).
[42] R. Lück, Qing Jiang, and B. Predel, J. Non-Cryst. Solids **117-118**, 911 (1990).
[43] T. Mizoguchi, S. Yoda, N. Akutsu, S. Yamada, J. Nishioka, T. Suemasa, and N. Watanabe, in *Rapidly Quenched Metals*, edited by S. Steeb and H. Warlimont (Elsevier, New York, 1985), p. 483.
[44] E. Matsubara and Y. Waseda, Mater. Trans., JIM **36**, 883 (1995).
[45] Y. Waseda, *The Structure of Non-Crystalline Materials* (McGraw-Hill, New York, 1980).
[46] T. Egami, K. Maeda, and V. Vitek, Philos. Mag. A **41**, 883 (1980); D. Srolovitz, K. Maeda, V. Vitek, and T. Egami, *ibid.* **44**, 847 (1981).
[47] V.V. Sokolovskij, *Theorie der Plastizität* (VEB-Verlag, Berlin, 1955).
[48] R. Busch, R. Schneider, S. Peker, and W.L. Johnson, Appl. Phys. Lett. **67**, 1544 (1995).
[49] D.R. Nelson and F. Spaepen, in *Solid State Physics*, edited by H. Ehrenreich and D. Turnbull (Academic Press, New York, 1989), Vol. 42, p. 1.